

1 **Scattering and Absorption Cross Sections of Atmospheric Gases in the**
2 **Ultraviolet-Visible Wavelength Range (307 - 725 nm)**

删除的内容: Cross-sections

3 Quanfu He¹, Zheng Fang¹, Ofir Shoshamin², Steven S. Brown^{3,4}, Yinon Rudich^{1,*}

4 ¹ Department of Earth and Planetary Sciences, Weizmann Institute of Science, Rehovot 76100,
5 Israel

6 ² Department of Environmental Physics, Institute for Biological Research, Ness-Ziona 74100,
7 Israel

8 ³ Chemical Sciences Division, Earth System Research Laboratory, National Oceanic and
9 Atmospheric Administration, 325, Broadway, Boulder, CO 80305, USA

10 ⁴ Department of Chemistry, University of Colorado, 216 UCB, Boulder, CO 80309, USA

11 *Correspondence to:* Yinon Rudich (yinon.rudich@weizmann.ac.il)

12

13 **Abstract**

14 Accurate Rayleigh scattering and absorption cross sections of atmospheric gases are essential for
15 understanding the propagation of electromagnetic radiation in planetary atmospheres. Accurate

删除的内容: cross-sections

16 extinction cross sections are also essential for calibrating high finesse optical cavities and
17 differential optical absorption spectroscopy and for accurate remote sensing. In this study, we

删除的内容: cross-sections

18 measured the scattering and absorption cross sections of carbon dioxide, nitrous oxide, sulfur
19 hexafluoride, oxygen, and methane in the continuous wavelength range of 307–725 nm using

删除的内容: cross-sections

20 Broadband Cavity Enhanced Spectroscopy (BBCES). The experimentally derived Rayleigh
21 scattering cross sections for CO₂, N₂O, SF₆, O₂, and CH₄ agree with refractive index-based

删除的内容: cross-sections

22 calculations, with a difference of (0.37±1.24)%, (-0.55±1.06)%, (0.91±1.35)%, (2.81±1.21)%, and
23 (0.89±2.18)%, respectively. The O₂-O₂ collision-induced absorption and absorption by methane

删除的内容: 1.5% and 1.1%, 1.5%, 2.9%, and 1.4% on average

24 are obtained with high precision at the 0.8 nm resolution of our BBCES instrument in the 307–725
25 nm wavelength range. New dispersion relations for N₂O, SF₆, and CH₄ were derived using data in

26 the UV-vis wavelength range. This study provides refractive index dispersion relations, *n*-based
27 Rayleigh scattering cross sections, and absorption cross sections for these gases.

删除的内容: improved

删除的内容: cross-sections, and absorption cross-sections

37 **1. Introduction**

38 The dominant interactions of gas-phase molecules with light in Earth’s atmosphere can be divided
39 into absorption, where the light energy is converted to internal energy and generally (at
40 atmospheric pressures) transferred to the surrounding environment either as heat or as
41 photoemission, and light scattering where the gases redistribute the light energy in the atmosphere.
42 The knowledge of light extinction (scattering + absorption) by gases is essential for predicting the
43 radiative transfer in the atmospheres of the Earth and other planets. In addition, the light extinction
44 by gases is widely used for determining the effective optical pathlength of high-finesse optical
45 cavities that measure trace gases and aerosols (Washenfelder et al., 2013; Washenfelder et al.,
46 2008; Wilmouth and Sayres, 2019; Jordan et al., 2019) and for Differential Optical Absorption
47 Spectroscopy (DOAS) to infer information about the light extinction properties of aerosols and
48 clouds in the open atmosphere (Baidar et al., 2013; Platt and Stutz, 2008).

49 The interaction of light with a wavelength much larger than the size of a molecule/particle gives
50 rise to the scattering of light, which is known as Rayleigh scattering (Strutt, 1899). Rayleigh
51 scattering accounts for scattering, local field effects (Lorentz–Lorenz) (Strutt, 1920) as well as
52 depolarization from the non-sphericity of molecule/particles (King correction factor) (King and
53 Eve, 1923; Strutt, 1918). For a gas with known refractive index (n_ν) and King correction factor
54 ($F_k(\nu)$), the wavelength-dependent Rayleigh scattering cross section (σ_ν , cm² molecule⁻¹) can be
55 calculated as follows (Sneep and Ubachs, 2005):

56
$$\sigma_\nu = \frac{24\pi^3 \nu^4}{N^2} \left(\frac{n_\nu^2 - 1}{n_\nu^2 + 2} \right)^2 F_k(\nu) \quad (1)$$

57 where N is the number density of the gas (molecules cm⁻³) and ν is the wavenumber of the light
58 (cm⁻¹). Note that the cross section contains the gas number density but is not in fact dependent on
59 the number density since the refractive index also appears in the expression. This n -based method
60 is an advantageous approach for calculating Rayleigh scattering cross sections, but it is vital to
61 note that the accuracy of the calculated cross sections depends on the experimentally-determined
62 refractive indices and the King correction factors. In particular, cautions should be used when
63 applying a dispersion formula derived from measurements in one wavelength region to calculate
64 Rayleigh scattering cross sections in a different wavelength range.

删除的内容: as

删除的内容: cross-section

删除的内容: cross-section

删除的内容:

删除的内容: cross-sections

删除的内容: cross-sections

删除的内容: index

删除的内容: cross-sections

73 Direct experimental measurement of Rayleigh scattering cross sections is essential given the
74 potential uncertainties in n -based calculations. While measurements of the King correction factors
75 and refractive index for gases are well known from the literature (Cuthbertson and Cuthbertson,
76 1932; Leonard, 1974; Strutt, 1920; Vukovic et al., 1996; Hohm, 1993), there are only a few direct
77 measurements of Rayleigh scattering cross sections (Fuchs et al., 2009; He et al., 2018; Ityaksov
78 et al., 2008a, b; Jordan et al., 2019; Naus and Ubachs, 2000; Sneep and Ubachs, 2005; Thalman
79 and Volkamer, 2013; Thalman et al., 2014; 2017; Wilmouth and Sayres, 2019; 2020), especially
80 measurements with a continuous spectrum from ultraviolet to visible.

删除的内容: cross-sections

81 Rayleigh scattering cross section measurements were previously performed at a single wavelength
82 (e.g., 458 nm, 532 nm, 632.8 nm) using Nephelometry (Shardanand and Rao, 1977) and cavity-
83 ring down spectroscopy (CRDS) (Ityaksov et al., 2008a, b; Naus and Ubachs, 2000; Sneep and
84 Ubachs, 2005; He et al., 2018). More recently, advanced Broadband Cavity Enhanced
85 Spectroscopy (BBCES) was used to determine the Rayleigh scattering cross sections of gases such
86 as Ar, CO₂, O₂, SF₆, and CH₄. The BBCES technique enables the measurement of Rayleigh
87 scattering cross sections over a broad wavelength range. Thalman et al. (2014) performed
88 measurements over selected wavelength regions between 350 and 660 nm using six BBCES
89 cavities for N₂, Ar, and O₂. The BBCES were calibrated with He and N₂ using Rayleigh scattering
90 cross sections calculated using their refractive index and from cavity-ring down measurements,
91 respectively. They found a good agreement with n -based values to within $0.2 \pm 0.4\%$. Recent studies
92 using BBCES with 30 nm spectral range were also used for Rayleigh scattering cross section
93 measurement in the UV wavelength region and demonstrated excellent agreement with n -based
94 values for Ar and CO₂ (Wilmouth and Sayres, 2020, 2019). Recently, Rayleigh scattering cross
95 sections for CO₂ were measured using BBCES at visible wavelengths between 400 and 650 nm,
96 and agreement with n -based values was within 2.4% on average. To the best of our knowledge,
97 there is no direct continuous wavelength measurements of extinction cross sections of gases that
98 covers the ultraviolet across the entire visible range (300–725 nm) as shown in Table 1. Recently,
99 Wilmouth and Sayres (2020) combined refractive index data in the UV region (264-297 nm and
100 333-363 nm) and at several single wavelengths in the visible, and they derived the dispersion
101 relation of refractive index for SF₆ and CH₄ in the wavelength range of 264-650 nm. However,
102 more data in the visible range are needed in order to further validate these dispersion relations.

删除的内容: cross-sections

删除的内容: ; He et al., 2018; Fuchs et al., 2009

删除的内容: cross-section

删除的内容: cross-sections

删除的内容: cross-sections

删除的内容: cross-sections

删除的内容: cross-section

删除的内容: cross-sections

删除的内容: cross-sections

113 In this study, we used a recently-developed BBCES instrument to measure the extinction cross
114 sections of CO₂, N₂O, SF₆, O₂, and CH₄ continuously across the wavelength region 307–725 nm.
115 All of the measurements were done at a single pressure to eliminate effects due to alignment.
116 This requires the use of two gases with different Rayleigh cross sections for the calibration of the
117 BBCES instrument since the reference state is not vacuum. In this study, He and N₂ were used to
118 calibrate the system. By using the *n*-based calculated Rayleigh scattering cross sections of He and
119 N₂ to calibrate the path length of the optical cavity, the other cross sections can be determined
120 relative to the difference between these two gases. We report high accuracy Rayleigh scattering
121 cross sections for all five gases and compared our results with previous *n*-based values. New
122 dispersion relations for N₂O, SF₆, and CH₄ are derived by incorporating data obtained by this study,
123 extinction cross section data in the deep UV, and previously available scattering cross section data
124 in the visible wavelength range.

删除的内容: cross-sections

删除的内容: cross-sections

删除的内容: cross-sections

删除的内容: cross-sections

删除的内容: cross-sections

删除的内容: cross-section

删除的内容: cross-section

125

126 2. Methods

127 2.1 Extinction measurement using BBCES

128 The BBCES systems used in this study are analogous to our previous studies (He et al., 2018;
129 Washenfelder et al., 2016; Bluvshstein et al., 2016). Briefly, our BBCES consists of two channels,
130 one in the UV (BBCES_{UV}, 307-350 nm) and one in the UV-vis range (BBCES_{vis}, 338-725 nm).
131 The two channels of the BBCES share a laser-driven Xenon arc lamp source (LDLS EQ-99CAL,
132 Energetiq Technology, Inc., MA, USA) coupled with a high transmission UV-Vis optical fiber
133 from which the light is collimated and focused (BBFIBERX-600-1M, Energetiq Technology, Inc.,
134 MA, USA). The light source was purged with high purity N₂ and cooled by an aluminum block
135 (with 15°C circulating water inside) to maintain stable optical power output. The UV light from
136 the fiber was reflected by a low-pass dichroic mirror and filtered (Schott Glass WG310 and UG11)
137 into the BBCES_{UV} channel, which has a cavity with two 2.5 cm diameter, 1 m radius of curvature
138 mirrors, with manufacturer's reported reflectivity of 0.9995 (per pass loss = 500 parts per million,
139 ppm) at the nominal center wavelength of 330 nm (Advanced Thin Films, Boulder, USA). The
140 transmitted UV-vis light from the beam splitter was reflected and filtered (Schott Glass WG345
141 and Edmund Optics 15-261) into the BBCES_{vis} channel consisting of two 2.5 cm, 1 m radius of
142 curvature mirrors (FiveNine Optics, USA) with manufacturer's reported reflectivity above 0.9993

删除的内容: is

删除的内容: is

152 (loss < 700 ppm), see Figure S1. The light emerging through the rear mirror of the cavity was
 153 focused using a 0.1 cm F/2 fiber collimator (74–UV, Ocean Optics, Dunedin, FL, USA) into a
 154 high transmission UV-vis optical fiber which directs the light into a high-performance
 155 spectrometer (QEPro, Ocean Insight, USA). Before gas measurement, the wavelength of the
 156 spectrometer was calibrated using an HG-1 mercury argon calibration light source (Ocean Insight,
 157 USA) within the wavelength range of 302.15–727.29 nm. During these experiments, a 300 line
 158 mm⁻¹ grating and a 200 μm entrance slit width were used. The CCD array is a back-illuminated
 159 detector with 1024×56 pixels (Hamamatsu S7031-1006, Japan) thermo-electrically cooled to -10 °C
 160 to reduce thermal noise. Individual spectra at a wavelength resolution of 0.8 nm were acquired
 161 with 3.0 s integration time, and a total of 150 spectra were recorded during each measurement.

162 During the extinction measurements, the entire 94.0 ± 0.1 cm pathlength between the mirrors was
 163 filled with He, N₂, CO₂, N₂O, SF₆, or CH₄. The gases were obtained from several vendors (Airgas,
 164 Linde) with the following purities: He, 99.995%; N₂, 99.999%; N₂O, 99.999%, CO₂, 99.999%;
 165 SF₆, 99.999%; CH₄, 99.9995%.

166 The reflectivity of the mirrors (R(λ)) can be determined as a function of wavelength (λ) by taking
 167 into account the difference in the extinction due to known literary data of Rayleigh scattering
 168 coefficient (α_{Ray}^{gas}) by two different gases such as N₂ (α_{Ray}^{N₂}(λ)) and He (α_{Ray}^{He}(λ)) (Washenfelder
 169 et al., 2008).

$$170 \quad R(\lambda) = 1 - d \frac{I_{N_2}(\lambda)(\alpha_{Ray}^{N_2}(\lambda)) - I_{He}(\lambda)(\alpha_{Ray}^{He}(\lambda))}{I_{He}(\lambda) - I_{N_2}(\lambda)} \quad (2)$$

171 where *d* is the length of the cavity filled by the gas. In this study, the studied gas filled the entire
 172 length of the cavity (94.0 ± 0.1 cm) since no purge flows were used. *I_{gas}* is the light intensity
 173 measured by filling the cavity with high purity N₂ (*I_{N₂}*(λ)) and He (*I_{He}*(λ)). Rayleigh scattering
 174 (α_{Ray}^{gas}) is the combined product of Rayleigh scattering cross section (σ) and the gas number density
 175 (*N*) during the measurements. Rayleigh scattering cross sections of N₂ and He were calculated
 176 using the data in Table 1. Figure S1 shows typical examples of light intensity when the BBCES
 177 cavities are filled with pure N₂. Reflectivity measurements were repeated every three sample
 178 measurements to track the stability of the system.

删除的内容: $\frac{1-R(\lambda)}{d}$

删除的内容:

删除的内容: cross-section

删除的内容: cross-sections

删除的内容: are

184 Once the reflectivity is determined, it is possible to calculate the wavelength-dependent extinction

185 cross sections of other gases ($\sigma(\lambda)$) as follows:

186
$$\sigma(\lambda) = \left[\left(\frac{1-R(\lambda)}{d} \right) \left(\frac{I_{He(\lambda)} - I_{gas(\lambda)}}{I_{gas(\lambda)}} \right) + \left(\frac{I_{He(\lambda)}}{I_{gas(\lambda)}} \right) \left(\alpha_{Ray}^{He}(\lambda) \right) \right] / N \quad (3)$$

187 Where N is the number density of the gas during the measurements, and $I_{gas}(\lambda)$ is the light intensity
188 when a target gas fills the cavity. During our experiments, the purge flow of the high reflection
189 mirrors was shut down to ensure that the cavity was filled with target gas completely. To measure
190 the extinction cross sections of CO₂, N₂O, and SF₆, the cavity is filled with pure target gas. Mass
191 flow controller controlled O₂/CH₄ flow was mixed with He in a 2 m Teflon tube ($\Phi = 1/4$ inch) to
192 generate a gas mixture with total flow rate of 500 mL min⁻¹. For O₂ experiments, measurements
193 were performed for O₂ + He mixtures by varying the O₂ percentage between 10% and 100% with
194 a 10% step. The CH₄ measurements were performed for CH₄ + He mixtures with CH₄ percentage
195 ranges between 10% to 100% with a 10% step. Additional measurements were also performed for
196 15%, 25%, 35%, and 45% CH₄.

197 **2.2 Extinction measurements using cavity-ring down spectroscopy (CRDS) at 404 nm and**
198 **662 nm.**

199 To obtain independent measurements for the extinction cross sections and to cross-validate of the
200 BBCES technique, we conducted CRD measurements at two fixed wavelengths of 404 nm and
201 662 nm. CRDS is a highly sensitive technique and uses a different measurement principle than
202 BBCES. The CRDS measured the decay rate of light due to extinction rather than an absolute
203 absorbance (as in the BBCES) and thus was immune to shot-to-shot source light fluctuations. A
204 detailed description of the CRD method for light extinction measurement can be found in
205 Bluvshstein et al. (2016) and He et al. (2018). Briefly, diode lasers (110 mW 404 nm diode laser,
206 iPulse, Toptica Photonics, Munich, Germany; 120 mW 662 nm diode laser, HL6545MG, Thorlabs
207 Inc., NJ, USA) were used as the light source of these CRDS. The 404 nm and 662 nm lasers were
208 modulated at 1383 Hz and 500 Hz with a 50% duty cycle. The diode lasers were optically isolated
209 by quarter waveplates ($1/4 \lambda$) and polarizing beam splitters to prevent damage to the laser head by
210 back reflections from the highly reflective CRDS mirror. The back-reflected light beam was
211 directed into a photodiode, which serves as an external trigger source. Light transmitted through
212 the back mirror of the cavity was collected by an optical fiber and detected by a photomultiplier

删除的内容: cross-sections

删除的内容: cross-sections

删除的内容: systems

删除的内容: cross-sections

删除的内容: validation

删除的内容: are

删除的内容: are

删除的内容: are

删除的内容: is

删除的内容: is

223 tube (PMT), which sampled at a rate of 10 to 100 MHz. The time-dependent intensity data was
224 acquired with a 100MHz card (PCI-5122, National Instruments, USA) and processed by data
225 acquisition software in Labview. An exponential curve was fitted to each intensity decay data set
226 (Figure S2). Over 1000 decay time measurements were monitored and averaged on a second basis.
227 The residual of the fit for the averaged intensity decay was obtained and further normalized to the
228 averaged intensity. The derived relative residuals (Figure S2) showed no apparent structure with
229 other time constants, validating the application of CRDS as a good measure of extinction. The
230 resultant 1 Hz decay time was averaged over one measurement duration of five minutes with
231 standard error as the measurement uncertainty.

删除的内容: s

删除的内容: is

删除的内容: is

删除的内容: are

删除的内容: is

删除的内容: is

232 All of the CRDS measurements were performed under room temperature and pressure downstream
233 from the BBCES instrument. The gas temperature (K-type thermocouple) and cavity pressure
234 (Precision Pressure Transducer, Honeywell International Inc., MN, USA) were recorded between
235 the two cavities for gas number density (N) calculation. During the CRDS measurements, the full
236 cavity was filled with the investigated gases (He, CO₂, N₂O, SF₆, O₂, CH₄, or gas mixtures (O₂ +
237 He and CH₄ + He)). The extinction cross section ($\sigma(\lambda)$) of the studied gas was measured relative
238 to that of He and was calculated by equation (4):

删除的内容: cross-section

$$239 \sigma(\lambda) = \frac{L}{cN} \left(\frac{1}{\tau_{gas}} - \frac{1}{\tau_{He}} \right) + \sigma_{He} \quad (4)$$

240 Where L is the total length of the cavity (l), c is the speed of light, and τ_{gas} and τ_{He} are the ring-down
241 time of the cavity when it is filled by target gas or by the reference gas, He.

242 2.3 Data processing

243 For comparison, the scattering cross sections of the gases investigated in this study were also
244 calculated with Equation (1) based on the refractive index and the King correction factors available
245 in the literature that are listed in Table 1. The King correction factors were taken as unity for mono-
246 atomic molecules and spherical molecules (with regards to the depolarization) but deviates for
247 non-spherical molecules. For the 307–725 nm wavelength range of this study, the n -based
248 calculated Rayleigh scattering cross sections from largest to smallest are SF₆ (Sneep and Ubachs,
249 2005; Wilmouth and Sayres 2020), N₂O (Sneep and Ubachs, 2005), CO₂ (Alms et al. 1975;
250 Bideau-Mehu et al. 1973), CH₄ (Sneep and Ubachs, 2005; Wilmouth and Sayres 2020), N₂ (Bates
251 1984), O₂ (Bates 1984; Sneep and Ubachs, 2005), and He (Abjean et al., 1970; Cuthbertson and

删除的内容: cross-sections

删除的内容: are

删除的内容: cross-sections

262 Cuthbertson, 1932). Additionally, the refractive indices of SF₆, N₂O, and CH₄ were calculated
263 based on Equation (1) using cross section results from this study and the King correction factors
264 listed in Table 1. Our measurements were performed under ~295K and ~1020 hPa. However, the
265 calculated refractive indices were scaled to 288.15K and 1013.25 hPa as in previous studies (Sneep
266 and Ubachs, 2005; Wilmouth and Sayres, 2020).

267 The extinction of O₂ + He mixtures (α_{O_2+He}) consists of the extinction by O₂ (α_{O_2}) and He (α_{He}),
268 and the O₂-O₂ collision-induced absorption ($\alpha_{O_2-O_2}$). The extinction of O₂ and He is a combined
269 product of extinction cross section (σ_{gas}) and gas number density (N_{gas}). Thus α_{O_2+He} can be
270 described with the following equation:

$$271 \alpha_{O_2+He} = \sigma_{O_2-O_2} \times N_{O_2}^2 + \sigma_{O_2} \times N_{O_2} + \sigma_{He} \times N_{He} \quad (5)$$

272 Where N_{O_2} and N_{He} are the number density of the O₂ and He in the cavities. Performing a 2nd order
273 polynomial fit to the extinction obtained by the BBCES with respect to the gas number density
274 thus yields the extinction cross section of O₂ and the O₂-O₂ collision-induced absorption (CIA)
275 cross section.

276 In addition to the results from 2nd order polynomial fitting, we also used data from pure O₂
277 measurement to calculate the extinction by O₂ and by CIA of O₂-O₂. The real refractive index of
278 O₂ (n_{O_2}) derived from extinction data measured in the wavelength regions where there is no
279 absorption was fitted using the generalized expression of $(n_{O_2} - 1) \times 10^8 = A + \frac{B}{C - \nu^2}$. Based
280 on the refractive index, the scattering cross sections of O₂ in the wavelength range of 307-725 nm
281 were further calculated. By subtracting the scattering cross section of O₂ from the measured total
282 extinction, we derived the CIA of O₂-O₂. However, the O₂ absorption bands at 580, 630, and 690
283 nm overlap with those of O₂-O₂ collisions. Additional corrections are thus needed to split the
284 absorption by O₂ and O₂-O₂ collision, which is out of the scope of this study.

285 Methane has weak vibrational overtone absorption in the UV-vis wavelength range that is
286 comparable to or greater than its Rayleigh scattering. Previous high-resolution spectroscopy
287 studies have identified smooth and unstructured absorption bands across the UV-visible range
288 (Giver, 1978; Smith et al., 1990). The spectral features are substantially broader than 0.8 nm, thus
289 the absorption by CH₄ can be measured by our BBCES. The measured extinction coefficients of

删除的内容: cross-section

删除的内容: cross-section

删除的内容: cross-section

删除的内容: cross-sections

删除的内容: cross-section

删除的内容: s

296 CH₄+He mixtures (α_{CH_4+He}) are linearly correlated with the number concentration of CH₄ (N_{CH_4})
297 as described by the following equation:

$$298 \alpha_{CH_4+He} = \sigma_{CH_4} \times N_{CH_4} + \sigma_{He} \times N_{He} \quad (6)$$

299 A linear fit was used for deriving the extinction cross section of CH₄. The absorption between 300
300 and 400 nm is negligible as compared to the Rayleigh scattering. Thus extinction data in this UV
301 wavelength range were used to calculate the real part of the refractive index of CH₄ which was
302 further fitted utilizing the expression of $(n_{CH_4} - 1) \times 10^8 = A + \frac{B}{C - \nu^2}$. By applying this
303 dispersion relation, the Rayleigh scattering cross sections in the entire wavelength range of 307–
304 725 nm were derived. Finally, the CH₄ absorption cross sections were calculated by subtraction of
305 the scattering cross section from the extinction cross section.

306 2.4 Error Propagation for Extinction Measurements

307 The uncertainty for BBCES measurements can be assessed by the propagation of the errors
308 associated with the measurements. Each parameter (temperature, pressure, light intensity) was
309 measured 150 times for each gas. The standard error of each parameter obtained from the 150
310 single measurements was used to calculate the uncertainty. The pressure ($\pm 0.01\%$), temperature
311 ($\pm 0.1\%$) and cavity length (94.0 ± 0.1 cm) are combined with the Rayleigh cross section
312 uncertainties for N₂ ($\pm 1\%$) as well as uncertainty in the measurements of the spectral signal by the
313 spectrometer ($\ll 0.2\%$) to get an overall relative uncertainty for the effective pathlength curve of
314 $\pm 1.03\%$. This uncertainty is further propagated to the target gas by consideration of the
315 uncertainties of pressure, temperature, and spectral intensity of the target gas measurements. The
316 overall 1- σ uncertainty of the gas extinction cross section is 1.1%. The precision of the mass flow
317 controllers is 0.5 mL min⁻¹. When the total flow rate is 500 mL min⁻¹, the resulting uncertainty in
318 the gas concentration (10-100%) varies from 0% to 1.0%. Thus, the overall 1- σ uncertainty of
319 extinction coefficients measured for CH₄+He and O₂+He varies from 1.1% to 1.5%. The detailed
320 wavelength-dependent uncertainties were calculated due to the wavelength-dependence of the
321 spectral intensity. The results are shown and discussed in later sections. The uncertainty for the
322 Rayleigh scattering cross section of N₂ is validated up to 468 nm. The uncertainty above this
323 wavelength may be larger than 1%, which is the value used for the calculation in our study. Thus,
324 the uncertainty at wavelengths longer than 468 nm may be underestimated. Moreover, due to the

删除的内容: the

删除的内容: cross-section

删除的内容: cross-sections

删除的内容: cross-sections

删除的内容: cross-section

删除的内容: cross-section

删除的内容: BBCES

删除的内容: cross-section

删除的内容: mirror reflectivity

删除的内容: cross-section

删除的内容: resulted

删除的内容: of

337 highly-structured reflectivity curve of the high-reflection mirrors, additional uncertainty could be
338 introduced and this uncertainty can not be quantified in this study.

339

340 **3 Results and Discussion**

341 **3.1 Performance of the optical system**

342 The reflectivity of the cavity mirrors, measured across the entire range using the difference in
343 Rayleigh scattering of N₂ and He, was very stable throughout the experiments. The measured
344 mirrors reflectivity curves are shown in Figure S1. The mean peak reflectivity of the BBCES_{UV}
345 mirrors was 0.999328 ± 0.000006 (672 ± 6 ppm) at 330 nm, with a corresponding effective optical
346 pathlength of 1.40 ± 0.01 km. The reflectivity curve of the BBCES_{vis} is much more structured, with
347 reflectivity ranging between 0.999224 ± 0.000010 and 0.9999550 ± 0.0000006 (776 ± 10 ppm > loss >
348 45 ± 0.6 ppm) over a wide wavelength range of 338–725 nm. The reflectivity of the BBCES_{vis} is
349 much higher than that of our previous system (He et al., 2018) and also covers a much broader
350 wavelength range. Thus the effective pathlength of the BBCES_{vis} varies between 1.3 and 20.4
351 km, guaranteeing a high sensitivity of the extinction measurement. The mean uncertainty in the
352 effective pathlength across the measured wavelengths as determined from the mirror reflectivity
353 was ±1.03%, which is predominantly due to the uncertainty in the Rayleigh scattering cross section
354 for N₂ derived from *n*-based calculation.

355 **3.2 Rayleigh scattering cross sections of CO₂, N₂O, SF₆.**

356 Figure 1 shows the extinction cross sections of CO₂, N₂O, and SF₆ measured by the BBCES. The
357 extinction cross sections of these gases monotonically decrease with increasing wavelength, and
358 no absorption (i.e., no structured extinction larger than the smoothly varying Rayleigh curve) is
359 observed in the wavelength range of 307–725 nm, indicating that the measured extinction is due
360 solely to the Rayleigh scattering of these gases. The wavelength-dependent relative standard
361 deviations of the measurements for each gas are shown in Figure 1d. The mean 1-σ uncertainty of
362 the reported cross sections for all three gases across the 307–725 nm wavelength range is 1.04%
363 for CO₂, 1.05% for N₂O, and 1.04% for SF₆. As mentioned above, the derived uncertainty
364 originates predominantly from the uncertainty in the N₂ Rayleigh scattering cross section.
365 Uncertainty in the Rayleigh cross sections of each gas varies with wavelength and generally tracks

删除的内容: cross-sections

删除的内容: cross-sections

删除的内容: cross-sections

删除的内容: 1.5% for CO₂, 1.1% for N₂O, and 1.5% for SF₆.

删除的内容: cross-section

删除的内容: cross-sections

373 the light intensity spectra, which is a combined product of light source spectrum and the mirror
374 reflectivity profile. The uncertainty is much higher when the transmitted light intensity is low
375 (Figure S1).

376 The BBCES measured Rayleigh scattering cross sections for these three gases agree well with
377 those obtained by our CRDS operating at 404 nm and 662 nm, with deviations smaller than 1.6%.

378 Table 2 listed the Rayleigh scattering cross sections at several wavelengths obtained by the BBCES
379 measurements (Exp) and by the calculations using the refractive index and $F_k(\nu)$ values from Table
380 1 (n -based). The relative differences between these two sets of results are within 1.4%.

381 Figure 1a–c shows a comparison of the measured Rayleigh scattering cross sections for CO₂, N₂O,
382 and SF₆ with n -based calculations and with previous experimental results from the literature. There
383 are a few measurements for the Rayleigh scattering cross sections for CO₂ which cover a wide
384 spectral range (Jordan et al., 2019; Shardanand and Rao, 1977; Snee and Ubachs, 2005; Wilmouth
385 and Sayres, 2019; He et al., 2018). There are fewer Rayleigh scattering measurements for N₂O and

386 SF₆ in the studied wavelength range. The measured Rayleigh scattering cross sections for CO₂,
387 N₂O, and SF₆ are in excellent agreement with n -based calculation. The wavelength-dependent
388 difference of our experimentally derived Rayleigh scattering cross sections with n -based
389 calculations are shown in Figure 1e. The mean ratios of our measurements to the n -based values
390 for the entire wavelength range of 307–725 nm are 1.00 ± 0.01 , 0.99 ± 0.01 , and 1.01 ± 0.01 for CO₂,

391 N₂O, and SF₆, respectively. The relative difference between our measurements and the n -based
392 values are $(0.37 \pm 1.24)\%$, $(-0.55 \pm 1.06)\%$, $(0.91 \pm 1.35)\%$ (Mean \pm SD) for CO₂, N₂O, and SF₆,
393 respectively. Variability of the relative difference is due to structure in the mirror reflectivity that
394 does not fully cancel. The wavelength-dependent Rayleigh scattering cross section is generally
395 described in the form of $\sigma = A \times \lambda^b$. In this study, the measured values and the n based data were
396 both fitted to this function. The relative difference between these two fitted functions is shown in
397 Figure 1(f). That would be a measure of the uncertainty comparing smooth functions to smooth
398 functions. The relative differences were $(0.49 \pm 0.48)\%$, $(-0.41 \pm 0.30)\%$, and $(0.94 \pm 0.22)\%$
399 (Mean \pm stdev), for CO₂, N₂O, and SF₆, respectively. The mean values of the relative difference
400 obtained from the fitting function are close to that obtained from the measurements. However, the
401 variabilities are much smaller, which may be related to the cancellation of the influence by the
402 structured mirror reflectivity. Notably, while our results for N₂O agree well with the n -based

删除的内容: cross-sections

删除的内容: cross-sections

删除的内容: theoretical

删除的内容: cross-sections

删除的内容: cross-sections

删除的内容: cross-sections

删除的内容: cross-sections

410 calculations, previous results obtained by CRDS at 532 nm (Sneep and Ubachs, 2005) and by
411 absorption spectroscopy in the wavelength of 300–315 nm (Bates and Hays, 1967) do not agree
412 well with the n -based calculations. The measurements between 300 and 315 nm were first
413 published by Bates and Hays (1967), who obtained the results from a doctoral thesis. However,
414 the results from our BBCES system are in good agreement with the n -based calculations and with
415 experimental results from independent CRDS measurements, thus increasing the confidence in our
416 measured values.

417 3.3 Scattering and absorption cross sections of O₂.

418 The UV-vis spectra of gas-phase molecular oxygen are characterized by discrete structured
419 absorption bands due to the electronic transition ($b^1 \Sigma_g^+(v' = 1/2/3) \leftarrow \Sigma_g^-(v'' = 0)$) of O₂
420 monomer, broader unstructured CIA of O₂–O₂, and structured dimer bands from the bound van
421 der Waals O₂ dimer (Newnham and Ballard, 1998). Under atmospheric conditions, the O₂–O₂ CIA
422 bands are frequently described as "O₄" bands, although absorption by O₂ dimer is thought to be
423 significant only under very low-temperature conditions (Thalman and Volkamer, 2013; Long and
424 Ewing, 1973). Within the wavelength range investigated in this work, the molecular oxygen B
425 band at 688 nm ($b^1 \Sigma_g^+(v' = 1) \leftarrow X^3 \Sigma_g^-(v'' = 0)$), γ overtone band at 629 nm ($b^1 \Sigma_g^+(v' = 2) \leftarrow$
426 $X^3 \Sigma_g^-(v'' = 0)$), and δ overtone band at 580 nm ($b^1 \Sigma_g^+(v' = 3) \leftarrow X^3 \Sigma_g^-(v'' = 0)$) overlap with
427 O₂–O₂ CIA bands of $^1 \Sigma_g^+(v = 1)$, $^1 \Delta_g + ^1 \Delta_g (v = 0)$, and $^1 \Delta_g + ^1 \Delta_g (v = 1)$, respectively.

428 These absorption bands can only be resolved by a high-resolution spectroscopic technique.

429 Absorption cross sections of the B, γ , and δ bands were convoluted from the HITRAN database
430 (Gordon et al., 2017) by considering the temperature, pressure, and wavelength resolution of the
431 instrument. The wings of the oxygen lines also show a quadratic dependence on the pressure due
432 to pressure broadening. However, due to the minimal O₂ absorption contribution below 680 nm

433 and the low instrument wavelength resolution, the extinction cross section of the O₂ monomer can
434 be treated as linearly correlated with the O₂ concentration. Moreover, the O₂–O₂ CIA cross section
435 is correlated with the square of the O₂ concentration. Therefore, these cross sections can be
436 retrieved from measurements at different O₂ concentrations. Due to the discrete structured

437 absorption bands and the wavelength resolution of the instrument, the range of absorption cross
438 sections spans several orders of magnitude within the spectral response of the instrument, limiting
439 the relevance of the absorption cross sections for other researchers. These results are not further

删除的内容: cross-sections

删除的内容: cross-sections

删除的内容: instrument's

删除的内容: cross-section

删除的内容: cross-section

删除的内容: cross-sections

删除的内容: instrument's

删除的内容: cross-sections

删除的内容: cross-sections

449 discussed here. However, the data for broader unstructured CIA of O₂-O₂ are still useful for
450 various applications.

451 Figure 2 shows the wavelength-dependent extinction coefficients of O₂+He mixtures. He was used
452 in these experiments to minimize extinction contributions from Rayleigh scattering. Nine
453 absorption peaks centered at 344 nm (CIA), 360 nm (CIA), 380 nm (CIA), 446 nm (CIA), 477 nm
454 (CIA), 532 nm (CIA), 577 nm (δ overtone and CIA), 629 nm (γ overtone and CIA), and 688 nm
455 (B band and CIA) were observed in the wavelength range of 307–725 nm. The absorption
456 coefficients of the central wavelengths for the first eight peaks increase non-linearly with O₂
457 concentration while that of the 688 nm peak increases in a more linear manner, indicating that the
458 O₂ B band absorption dominates the last absorption peak while the other peaks are mostly
459 associated with CIA of O₂-O₂.

460 The extinction coefficients obtained by the BBCES correlated well with those measured by the
461 CRD, with slopes of 0.990 ($R^2=0.9994$) and 0.993 ($R^2 = 0.9996$) at the wavelengths of 404 nm and
462 662 nm, respectively (Figure 3). This excellent agreement between the instruments further
463 substantiates the BBCES measurements and suggests that the accuracy of the BBCES at these two
464 wavelengths is better than estimated in the error propagation above, where the N₂ refractive index
465 was the largest uncertainty. As explained in the data processing section, the measured extinction
466 coefficients were fitted with a 2nd order polynomial (selected wavelengths at the peaks of the CIA
467 absorption bands are shown in Figure 4). At 476.7, 577.2, and 629.2 nm, the absorption is from
468 the CIA of O₂-O₂. The fit generates positive values matching the absorption cross section of O₂-
469 O₂ CIA. At 687.7 nm where strong B-band absorption appears, the fit yields a small negative
470 coefficient for O₂-O₂ CIA.

471 Figure 5a shows the extinction cross section measured for 100% O₂. These results agree well with
472 previously reported results by Jordan et al. (2019). For wavelengths where no absorption is
473 detected, the measured extinction cross sections agree well with *n*-based calculations. Figure 5b-c
474 shows the determined extinction cross sections for molecular O₂ and the absorption cross sections
475 of O₂-O₂ CIA. For wavelength ranges without O₂ bands, our extinction cross sections agree well
476 with the *n*-based values with an average deviation of (2.81±1.21)%. The absorption cross sections
477 for O₂-O₂ CIA derived in this study mostly agree well with literature data from Thalman and
478 Volkamer (2013). The differences are within 1.1% at 477, 532, 577, and 630 nm but larger

删除的内容: cross-section

删除的内容: cross-section

删除的内容: cross-sections

删除的内容: cross-sections

删除的内容: cross-sections

删除的内容: cross-sections

删除的内容: 2.8

删除的内容: cross-sections

487 deviations were found at 344 (4.2%), 360 (-29%), 380 (-21%), and 446 (4.2%) nm. These
488 absorption bands are the lowest intensity bands and therefore have the largest relative uncertainties
489 in either measurement. Moreover, the absorptions at 344, 360, 380, and 446 nm contribute a much
490 smaller fraction of the extinction as compared to that of 477, 532, 577, and 630 nm. Thus larger
491 discrepancies were observed during the apportionment of absorption from extinction.

492 The Rayleigh scattering cross sections of molecular O₂ derived from the 100% O₂ measurement
493 agree well with *n*-based calculations with an average difference of 1.2%. CIA of O₂-O₂ calculated
494 from this single measurement matches the results from the fitting method. Due to strong absorption
495 from O₂ B band and γ overtone band, this method cannot derive the cross sections of CIA of O₂-
496 O₂ at 630 and 688nm.

497 3. 4 The scattering and absorption cross sections of CH₄.

498 CH₄ has weak absorption in the UV-vis wavelength range, and these bands dominate the
499 photographic spectra of planets such as Uranus and Neptune (Adel and Slipher, 1934). Figure 6
500 presents the wavelength-dependent extinction coefficients of CH₄+He mixtures. A total of eleven
501 absorption bands were detected in the wavelength range of 307-725 nm. The extinction
502 coefficients increase as a function of increasing CH₄ concentration. Extinction coefficients
503 obtained by the BBCES correlated well with those measured in parallel by the CRDS, with slopes
504 of 1.002 ($R^2=0.9999$) and 0.99 ($R^2 = 0.999$) at the wavelengths of 404 nm and 662 nm (Figure S3).
505 The excellent agreement between these three systems further supports the accuracy of BBCES
506 extinction measurements over a wide working range. The measured extinction coefficients were
507 linearly fit against the CH₄ number concentration. Figure 7 shows the fitted curves at five selected
508 wavelengths. The extinction coefficients have a linear correlation with CH₄ concentration ($R^2 >$
509 0.9988) without exception. The calculated slopes represent the extinction cross sections of CH₄
510 and also indicate a wide dynamic range of our BBCES.

511 The extinction cross sections for CH₄ retrieved from concentration-dependent measurements are
512 plotted in Figure 8a. BBCES results from this study agree well with results from previous studies
513 using BBCES (Jordan et al., 2019; Wilmouth and Sayres, 2019) and CRDS (Sneep and Ubachs,
514 2005). Previous studies using a Nephelometer (Shardanand and Rao, 1977) and interferometer
515 (Cuthbertson and Cuthbertson, 1920; Watson et al., 1936) obtained the scattering cross sections
516 and the refractive index of CH₄. The BBCES measures the extinction cross section. For

删除的内容: cross-sections

删除的内容: cross-sections

删除的内容: cross-sections

删除的内容: cross-sections

删除的内容: cross-sections

删除的内容: cross-sections

删除的内容: cross-section

524 wavelengths where extinction is dominated by Rayleigh scattering (< 475 nm), our BBCES results
 525 agree well with the results from Nephelometer and interferometer measurements. In this study, the
 526 refractive index of CH₄ was calculated using the extinction data in the wavelength range of 307-
 527 400 nm. The calculated refractive index was fitted to the general expression:

$$528 \quad (n_{CH_4} - 1) \times 10^8 = 5476 + \frac{4.1579 \times 10^{14}}{1.1568 \times 10^{10} - \nu^2} \quad (7)$$

529 As shown in Figure 8b, our calculated scattering cross sections are in good agreement with those
 530 derived from the newest refractive index developed by Wilmouth and Sayres (2020) (Table 2),
 531 with an average difference of (0.89 ± 2.18)%. The absorption cross section, which is the difference
 532 between the total extinction and the Rayleigh scattering cross section, is shown in Figure 8c. At
 533 most spectral ranges, our results are in better agreement with the results from previous studies by
 534 Giver, (1978) and Smith et al.(1990). For example, the difference as compared to the results from
 535 Giver (1978) at 542, 576.4, 598, 619, 665.7, and 703.6 nm is 4.0% on average. At several
 536 wavelength regions (e.g., 520–536nm, 580–605 nm), the results from Fink et al. (1977) differ from
 537 all of the other studies. In the wavelength range of 400–725 nm, absorption contributes up to 99.7%
 538 of the CH₄ extinction.

539 3. 5 Dispersion relations for N₂O, SF₆ and CH₄.

540 **SF₆:** Wilmouth and Sayres (2020) found that their measured Rayleigh scattering cross sections for
 541 SF₆ in the ultraviolet range were lower than those from the *n*-based expression of Sneep and
 542 Ubachs (2005). They generated the dispersion formula for SF₆ from the combined fit using
 543 refractive index data in the wavelength range of 264-297 nm and 333-363 nm by Wilmouth and
 544 Sayres (2020, 2019), and direct refractive index measurement at 632.99 nm (Vukovic et al., 1996)
 545 (Figure 9a). In our study, the refractive index of SF₆ in the wavelength range of 307-725 nm was
 546 calculated from the measured Rayleigh scattering cross section for 288.15 K and 1013.25 hPa. To
 547 better constrain the dispersion formula when extrapolated over a broad wavelength range, we
 548 employed an alternative fit of the form A+B/(C-ν²) to our data and the data used by Wilmouth and
 549 Sayres (2020) for fitting. All sets of data were weighted equally. The resulting dispersion relation
 550 for SF₆ in the wavelength range of 264–725 nm is

$$551 \quad (n_{SF_6} - 1) \times 10^8 = 18997.7 + \frac{8.27663 \times 10^{14}}{1.56833 \times 10^{10} - \nu^2} \quad (8)$$

删除的内容: cross-sections

删除的内容: 1.4

删除的内容: cross-section

删除的内容: cross-section

删除的内容: good

删除的内容: (Giver, 1978; Smith et al., 1990)

删除的内容: cross-sections

删除的内容: much

已下移 [1]: To better constrain the dispersion formula when extrapolated over a broad wavelength range, we employed an alternative fit of the form $A+B/(C-\nu^2)$ to our data.

删除的内容: To better constrain the dispersion formula when extrapolated over a broad wavelength range, we employed an alternative fit of the form $A+B/(C-\nu^2)$ to our data. The Rayleigh scattering derived

删除的内容: were used

已移动(插入) [1]

删除的内容: $(n_{SF_6} - 1) \times 10^8 = 22871 + \frac{8.0021 \times 10^{14}}{1.6196 \times 10^{10} - \nu^2}$

569 **N₂O**: Sneep and Ubachs (2005) derived the refractive index based on polarizability measurements
 570 using interferometer at five single wavelengths (457.9, 488, 514.5, 568.2, 647.1 nm) by Alms et
 571 al. (1975). In this study, we calculated the refractive index of N₂O from the Rayleigh scattering
 572 cross sections in the wavelength range of 307–725 for 288.15K and 1013.25 hPa. Based on this
 573 refractive index data set, the dispersion relation (Eq (9)) for N₂O was retrieved for a much broader
 574 wavelength range (Figure 9b) compared to that generated by Sneep and Ubachs (2005).

删除的内容: cross-sections

$$575 (n_{N_2O} - 1) \times 10^8 = 22095 + \frac{1.66291 \times 10^{14}}{6.75226 \times 10^9 - \nu^2} \quad (9)$$

删除的内容: $(n_{N_2O} - 1) \times 10^8 = 23154 + \frac{1.534 \times 10^{14}}{6.5069 \times 10^9 - \nu^2}$

576 **CH₄**: The previous study by Wilmouth and Sayres (2019) has shown that their measured Rayleigh
 577 scattering cross sections for CH₄ are in substantial disagreement (22%) with those calculated from
 578 the refractive index recommended by Sneep and Ubachs (2005). Sneep and Ubachs (2005)
 579 formulated the refractive index of CH₄ based on interferometric measurements at wavelengths of
 580 325, 543.5, 594.1, 612, and 633 nm by Hohm (Hohm, 1993). However, the Rayleigh scattering
 581 cross sections calculated from their refractive index are much higher than all the measured values
 582 listed in Figure 9b. Using equally weighted Rayleigh scattering cross sections data sets in the
 583 wavelength range of 264–297 nm, 333–363 nm (Wilmouth and Sayres, 2019, 2020), 307–400 nm
 584 from this study, and single wavelength measurements that are not impacted by absorption
 585 (Cuthbertson and Cuthbertson, 1920; Watson et al., 1936), we derived the dispersion formula for
 586 the refractive index of CH₄ in the combined UV/visible range (Figure 9c) as follows:

删除的内容: cross-sections

删除的内容: cross-sections

删除的内容: cross-sections

删除的内容: which

删除的内容: ; Shardanand and Rao, 1977

$$587 (n_{CH_4} - 1) \times 10^8 = 3603.09 + \frac{4.40362 \times 10^{14}}{1.1741 \times 10^{10} - \nu^2} \quad (10)$$

删除的内容: $(n_{CH_4} - 1) \times 10^8 = 7327.7 + \frac{4.1884 \times 10^{14}}{1.2208 \times 10^{10} - \nu^2}$

588 The calculated Rayleigh scattering cross sections using the dispersion relations derived in this
 589 study were compared with those derived from previously recommended formulations listed in
 590 Table 1 (Figure 9). The difference increases significantly towards the longer wavelength in the
 591 region of 320–725 nm (Figure S4). The average deviations are 0.1%, 0.9%, and 0.1% for SF₆, N₂O,
 592 and CH₄, respectively. Notably, the difference for N₂O is more significant than for the other two
 593 gases. This study uses refractive index data in the continuous wavelength ranges of 307–725 nm
 594 to derive the dispersion relation, while the formulation for N₂O in Table 1 is derived by Sneep and
 595 Ubachs (2005) based on polarizability measurements at five single wavelengths. For the
 596 formulation of the refractive index of CH₄, Wilmouth and Sayres (2020) weighted the data sets
 597 from Watson and Ramaswamy (1936) and Cuthbertson and Cuthbertson (1920) equally but gave

删除的内容: cross-sections

删除的内容: at

删除的内容: 0.8

删除的内容: 1.6

删除的内容: Notably, the difference for CH₄ is much more significant than for the other two gases. This study uses additional measurements and literature data in the wavelength ranges of 307–333nm and 363–400 nm than those used by Wilmouth and Sayres (2020).

615 more weight to their UV measurements when deriving the formulation of the refractive index. In
616 this study, all the CH₄ data set were weighted equally. The derived dispersion relation agrees very
617 well with that from Wilmouth and Sayres (2020), as shown in Figure 9 (c-d).

618 **Conclusions and Implications**

619 Rayleigh scattering cross sections between 307 and 725 nm were determined for CO₂, N₂O,
620 SF₆, O₂, and CH₄ by simultaneous BBCES and CRDS measurements. Extinction coefficients
621 obtained by the BBCES show high consistency with those measured by parallel CRDS at 404 and
622 662 nm (Figure 3 and figure S3), demonstrating that the BBCES measurements provide results
623 with both a wide wavelength range and high accuracy. Comparison of our measurements with the
624 n-based calculations for these gases in the entire wavelength range of this study yields excellent
625 agreement with relative differences of (0.37±1.24)%, (-0.55±1.06)%, (0.91±1.35)%,
626 (2.81±1.21)%, and (0.89±2.18)%, respectively. The O₂-O₂ CIA cross sections obtained from the
627 BBCES measurements are compared with those published by Thalman and Volkamer (2013). The
628 relative differences are within 1.1% at 477, 532, 577, 630 nm. Larger relative differences occur at
629 the weak bands at 344 (4.2%), 360 (-29%), 380 (-21%), and 446 (4.2%) nm. The absorption cross
630 sections of CH₄ in the wavelength range of 400-725 nm agree well with those documented by
631 Giver (1978).

632 Rayleigh scattering cross sections of CO₂ determined using BBCES and CRDS in this study,
633 and in other studies have shown that the refractive index recommended by Snee and Ubachs
634 (2005) is suitable for use in the wavelength range of 307–725 nm. By incorporating the refractive
635 index data from previous studies, we developed new dispersion relations for the refractive index
636 of N₂O (307-725 nm), SF₆ (264–725 nm), and CH₄ (264–671 nm). The derived dispersion relations
637 for SF₆ and CH₄ agree well with those provided by Wilmouth and Sayres (2020).

638 Previous studies measured the Rayleigh scattering and absorption cross sections of CO₂, N₂O,
639 O₂, SF₆, and CH₄ at narrow spectral ranges or single wavelengths. In this study, we used BBCES
640 that covers the broad wavelength range of 307–725 nm to measure total extinction (the sum of
641 absorption and scattering). The measurements validate that refractive index-based methods for
642 calculating Rayleigh extinction cross sections are accurate and provide new fits over more
643 continuous and extended wavelengths range than available in the literature to constrain such
644 methods. The Rayleigh scattering cross sections reported here are useful in several applications.

删除的内容: Therefore this fit captures well our BBCES measurements (Figure 9d), and also the Wilmouth and Sayres (2020, 2019) data. .

删除的内容: cross-sections

删除的内容: 1.5% and 1.1%, 1.5%, 2.9%, and 1.4% on average

删除的内容: cross-sections

删除的内容: cross-sections

删除的内容: cross-sections

删除的内容: The new dispersion relation for CH₄ captures the measurements from BBCES more adequately

删除的内容: cross-sections

删除的内容: cross-sections

删除的内容: cross-sections

659 These include calibration standards based on extinction for optically-based instruments, such as
660 those designed for aerosol optical properties measurements or trace gas concentrations in the field
661 (Jordan et al., 2019; Min et al., 2016; Bluvshstein et al., 2017), especially when high-refractive
662 index gases are used for improved calibration. They will also improve the accuracy of Rayleigh
663 scattering parameterizations for major greenhouse gases in Earth's atmosphere, CO₂, CH₄, and
664 N₂O. Accurate quantitative measurements of Rayleigh scattering coefficients and absorption ~~cross~~
665 ~~sections~~ of atmospheric gases such as molecular N₂, O₂, CO₂ and the CIA of O₂-O₂ ~~cross sections~~
666 in the UV-NIR range are of particular importance for the application of Rayleigh LIDAR systems,
667 especially at the Nd:YAG laser harmonics 1064, 532 & 366 nm. These systems analyze the
668 molecular backscattering contributions to the LIDAR's attenuated backscatter signals to retrieve
669 the atmospheric profile of aerosols and clouds in the planetary boundary layer (Tomasi et al., 2005;
670 Herron, 2007). Recent NASA satellite missions have also aimed to measure global carbon dioxide
671 concentrations with high precision (0.25%) (Drouin et al., 2017). These CO₂ global missions use
672 the O₂-O₂ CIA underneath the structured O₂ A-band (760 nm) to evaluate the solar radiation
673 double pathlength in the Earth atmosphere and to determine the atmospheric pressure. The
674 measurements in this study validate the existing literature on the extinction of O₂ collision
675 complexes and molecular oxygen bands, and can be used for calibration purposes in both remote
676 sensing and *in-situ* spectroscopic applications in the atmosphere. In the future, gas extinction
677 measurements at extended wavelengths (near-infrared) and for additional gases (e.g., N₂) will
678 improve the spectroscopic applications in atmospheric studies.

679 **Data availability.**

680 Data are available upon request from the corresponding author (yinion.rudich@weizmann.ac.il).

681 **Author contributions.**

682 Q.H., S.S., and Y.R. designed this study. Q.H., Z.F., and O.S. conducted the experiments. Q.H.
683 prepared the draft and all of the co-authors reviewed it and provided comments.

684 **Competing interests.**

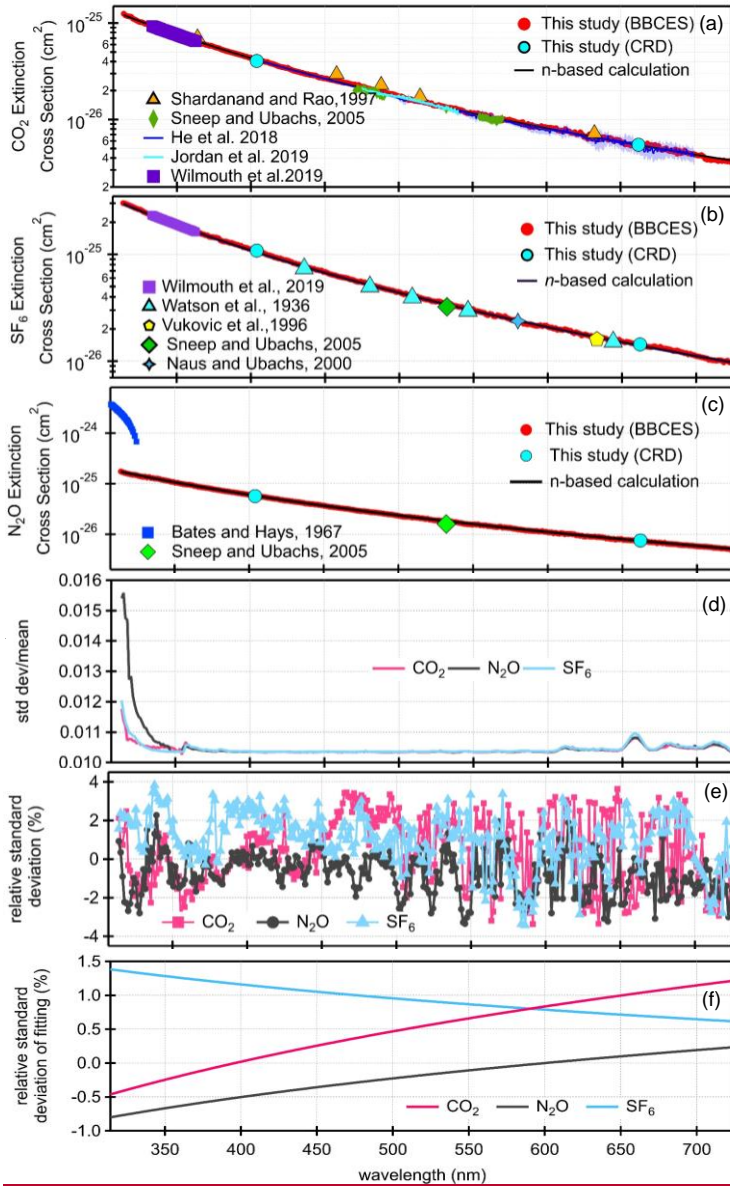
685 The authors declare that they have no conflict of interest.

686 **Acknowledgments**

删除的内容: cross-sections

删除的内容: cross-sections

689 This research was partially supported by the US-Israel Binational Science Foundation (BSF grant
690 #2016093). Dr. Q. H. is supported by the Koshland Foundation and the Center for Planetary
691 Sciences, Weizmann Institute of Science. Dr. Z.F. is supported by SAERI initiative of the
692 Weizmann Institute.



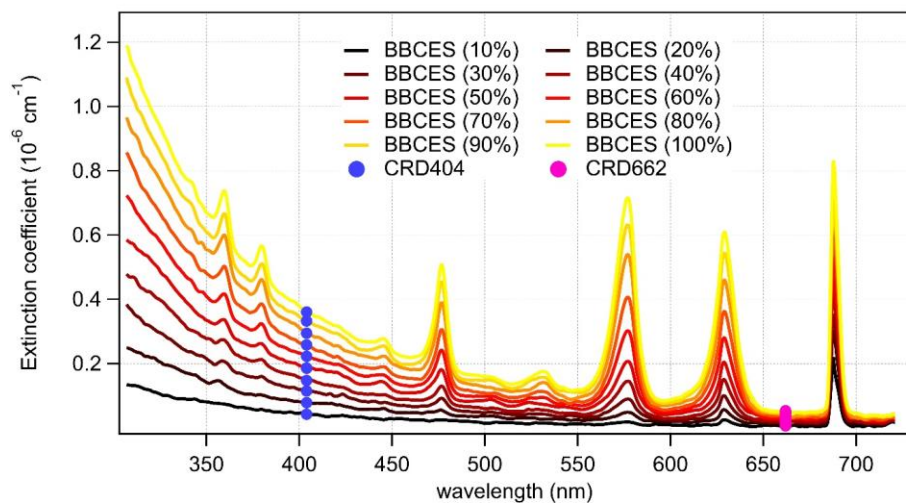
693
 694 Figure 1. Rayleigh scattering cross sections of CO₂ (a), SF₆ (b), and N₂O (c). Panel (d) shows the
 695 relative standard deviations as a function of wavelength for each gas. The relative difference in the

删除的内容: cross-sections

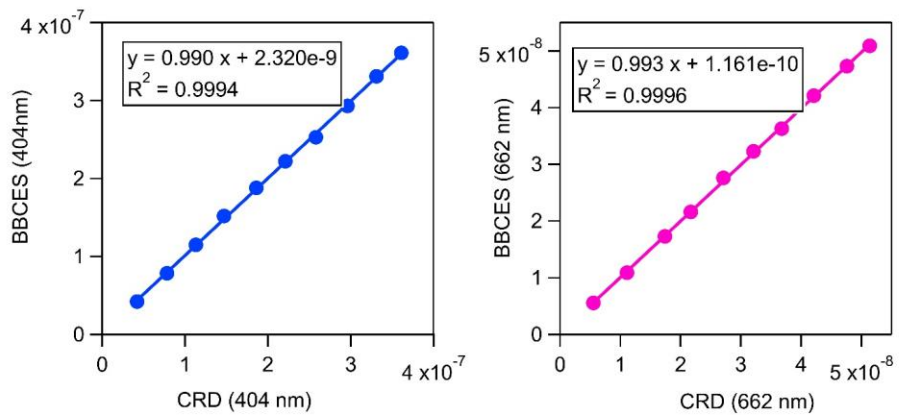
697 cross sections obtained by our measurements and calculations from the refractive index are
698 displayed (e). Panel (f) shows the relative difference after fitting ($\sigma=A\lambda^B$).

删除的内容: cross-sections

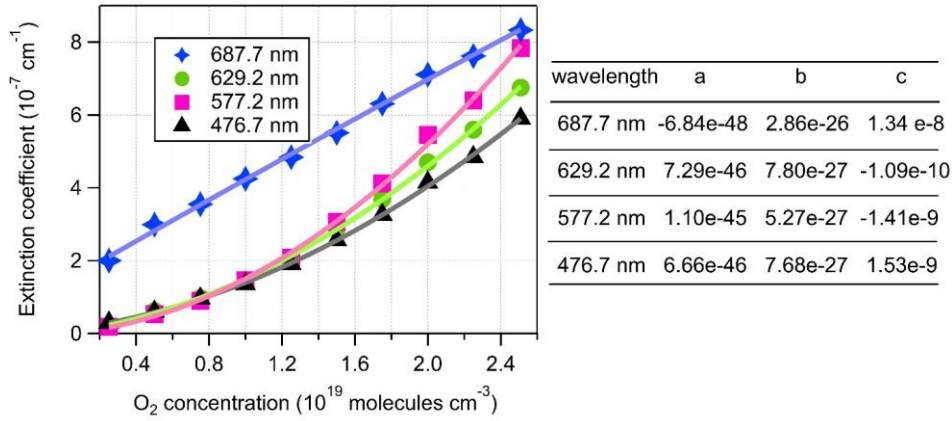
删除的内容: the BBCES



699
700 Figure 2. Wavelength-dependent extinction coefficients of O₂ + He mixtures as a function of O₂
701 concentration. The colored lines represent the extinction coefficients measured by BBCES, and
702 markers represent results from CRDS.



705
 706 Figure 3. Correlations between the extinction coefficients (unit, cm⁻¹) measured by the BBCES
 707 and CRDS.

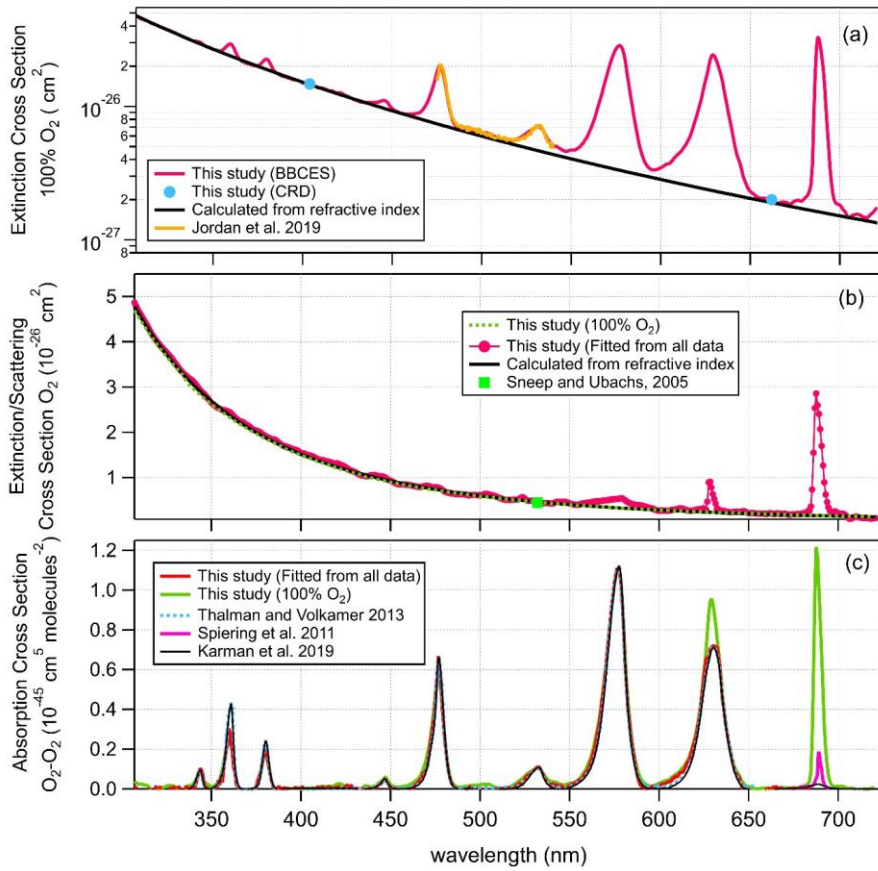


708

709 Figure 4. 2nd order polynomial fit of extinction coefficients measured by the BBCES. The O₂
 710 concentration-dependent extinction coefficients are contributed by the extinction coefficients of
 711 O₂ (σ_{O_2}), He (σ_{He}), and the O₂-O₂ CIA cross sections ($\sigma_{O_2-O_2}$).

删除的内容: cross-sections

带格式的: 字体: (默认) Times New Roman, 小四



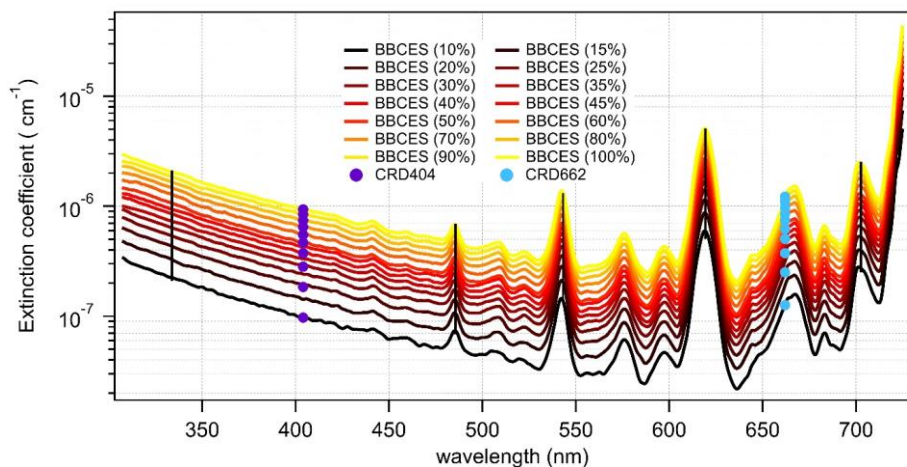
713

714 Figure 5. Wavelength-dependent extinction cross sections of 100% O₂ (a), extinction cross
715 sections of O₂ (b), and O₂-O₂ CIA cross section (c).

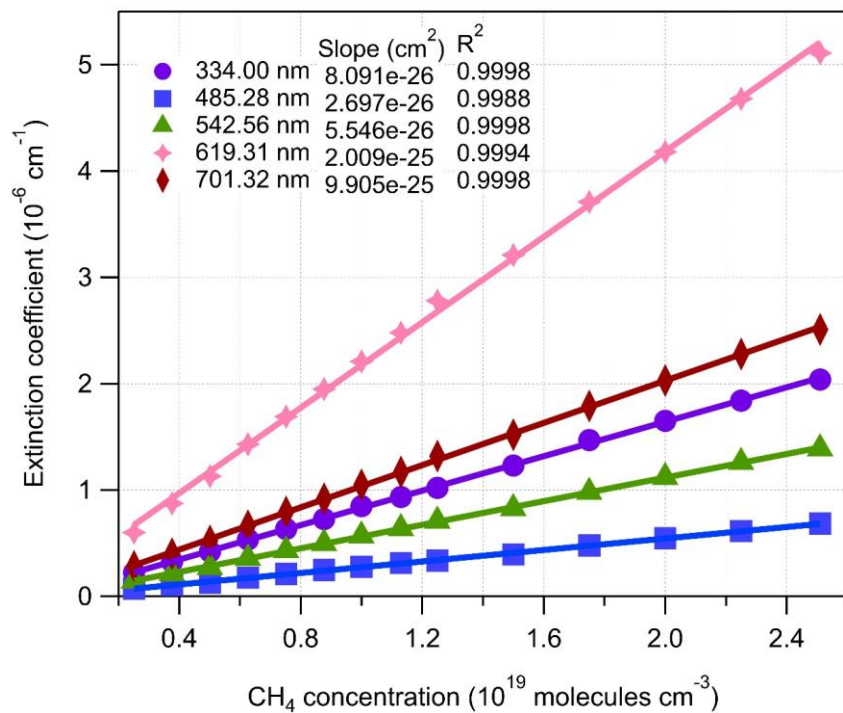
删除的内容: cross-sections

删除的内容: cross-sections

删除的内容: cross-section

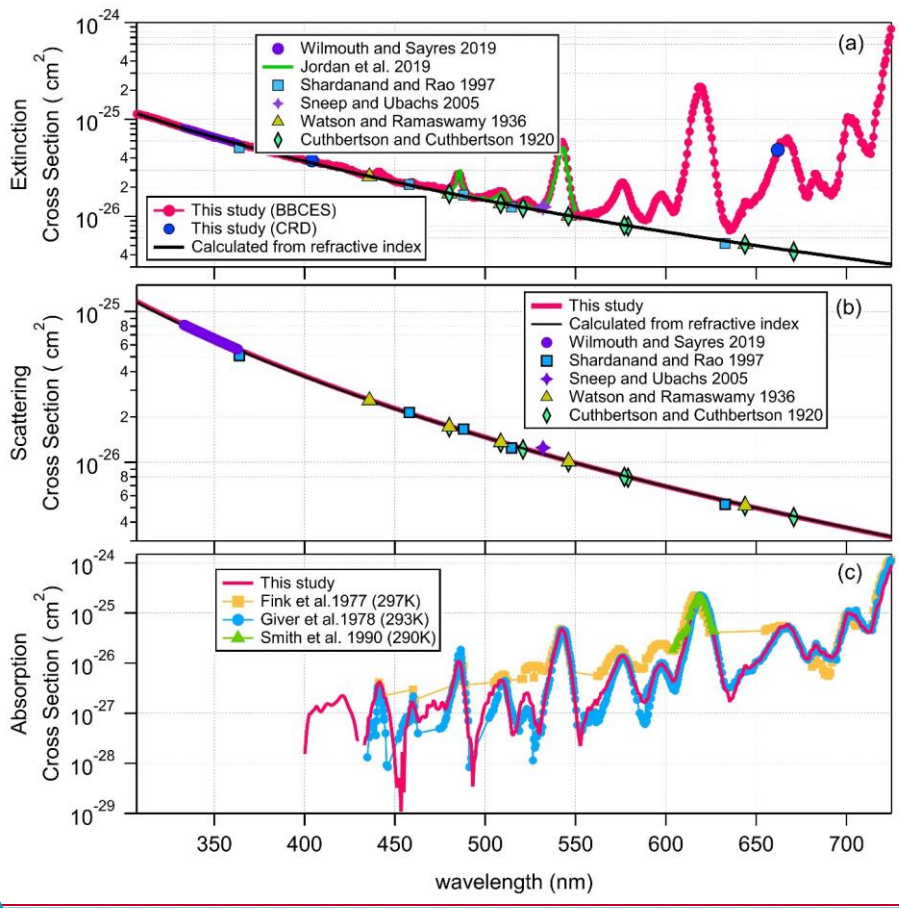


719
 720 Figure 6. Wavelength-dependent extinction coefficients of CH₄ + He mixtures as a function of
 721 CH₄ mixing ratio. The colored lines represent extinction coefficients obtained from BBCES and
 722 markers represent results from CRDS. Measurements were performed with CH₄ percentage within
 723 10% and 100% with a 10% step. Moreover, BBCES measurements were also performed for 15%,
 724 25%, 35%, and 45% CH₄. The number concentration of 100% methane was 2.50143×10^{19}
 725 molecules cm⁻³. Data at selected wavelengths (vertical lines) are shown in Figure 7.



726
 727 Figure 7. The relationship between BBCES measured extinction coefficients of CH₄+He mixtures
 728 and CH₄ concentration. The selected wavelengths were located in Figure 6 by vertical lines.

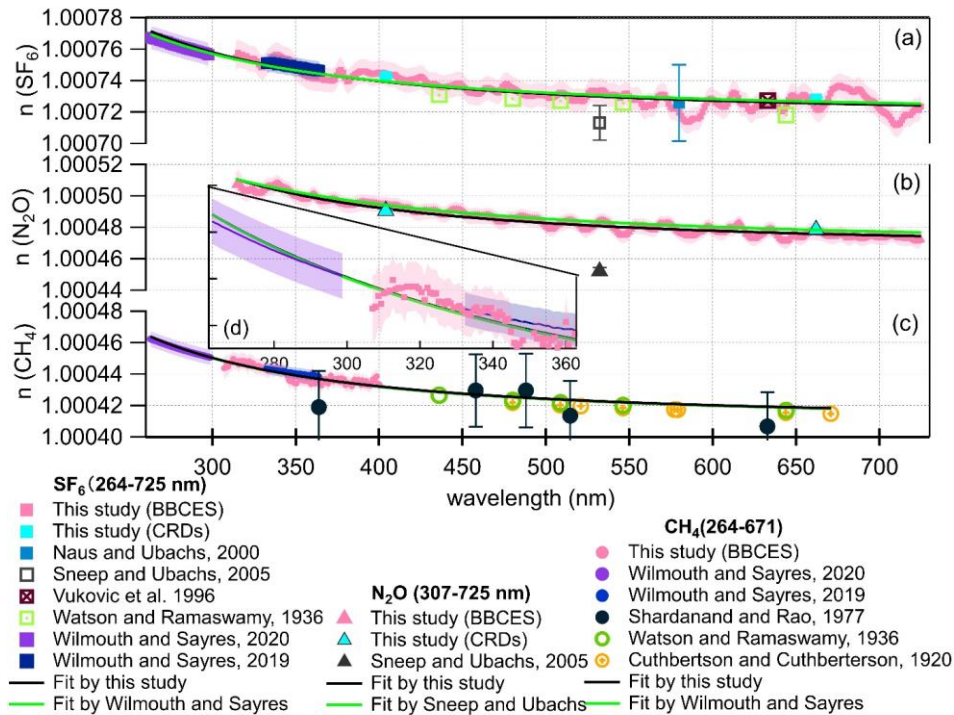
带格式的: 字体: (默认) Times New Roman, 小四



729

730 Figure 8. Extinction (a), scattering (b), and absorption (c) cross sections of CH₄.

删除的内容: cross-sections



732
 733 Figure 9. Real refractive index (n) for SF_6 (a), N_2O (b), and CH_4 (c). Comparison of Refractive
 734 index from this work with previous studies (Cuthbertson and Cuthbertson, 1920; Naus and Ubachs,
 735 2000; Shardanand and Rao, 1977; Sneep and Ubachs, 2005; Vukovic et al., 1996; Watson et al.,
 736 1936; Wilmoth and Sayres, 2019, 2020) over the wavelength range of 264–725 nm. The green
 737 line represents the dispersion relation given in Table 1. The black line represents the dispersion
 738 relation given in Eq. (8–10) derived from a fit to our data and references results. The shading
 739 represents 1- σ uncertainty of the n . The n values for Shardanand and Rao (1977), Sneep and
 740 Ubachs (2005), Naus and Ubachs (2000) were calculated from their reported Rayleigh scattering
 741 cross sections. Refractive index data from Sneep and Ubachs (2005) are not used in the fitting
 742 since these results are away from others. Data from Shardanand and Rao (1977) are not used due
 743 to large uncertainties. All of the data sets are equally weighted during fitting. Panel (d) is a close-
 744 up view of panel (c) in the wavelength range of 264–363 nm.

删除的内容: cross-sections

删除的内容: the

删除的内容: .

748 Table 1. Refractive index and King correction factors for calculating Rayleigh scattering cross-
 749 sections and available measurements in the wavelength range of 300–725 nm. Measurements for
 750 He and N₂ are not summarized in this table.

Gas	Refractive index and King correction factors			Measurements		
	$(n-1) \times 10^8$	$F_K(v)$	ν (cm ⁻¹)	References	λ (nm)	References
He	2283 + $\frac{18102 \times 10^{13}}{1.5342 \times 10^{10} - \nu^2}$	1.0	14285- 33333	<i>Abican, 1970;</i> <i>Leonard, 1974;</i> Cuthbertson, 1932		
N ₂	5677.465 + $\frac{318.81874 \times 10^{12}}{1.44 \times 10^{10} - \nu^2}$	1.034 + 3.17 × 10 ⁻¹² ν ²	21360- 39370	<i>Bates 1984</i> Sneep, 2005; Naus, 2000		
CO ₂	$\frac{1.1427 \times 10^{11}}{5799.25}$ × $\left(\frac{128908.9}{120.05}\right)^2 - \nu^2$ + $\frac{5.3334}{(89223.8)^2 - \nu^2}$ + $\frac{4.3244}{(75037.5)^2 - \nu^2}$ + $\frac{4.3244}{(67837.7)^2 - \nu^2}$ + $\frac{1.218145 \times 10^{-5}}{(2418.136)^2 - \nu^2}$	1.1364 + 2.53 × 10 ⁻¹¹ ν ²	39417- 55340	<i>Alms, 1975;</i> <i>Bideau-Mehu,</i> <i>1973;</i> Sneep, 2005	333-725	Jordan, 2019; Shardanand, 1977; Sneep, 2005; Wilmouth, 2019; He, 2018
CH ₄	4869.8 + $\frac{4.1023 \times 10^{14}}{1.133 \times 10^{10} - \nu^2}$	1.0	15385- 40000	<i>Sneep, 2005;</i> <i>Wilmouth, 2020</i>	<i>264-297</i> 333-363, 434-725	Cuthbertson 1920; Jordan, 2019; Shardanand, 1977; Sneep, 2005; Watson, 1936; Wilmouth, 2019; 2020 ; Smith, 1990; Giver, 1978; Fink, 1977
N ₂ O	46890 + 4.12 × 10 ⁻⁶ ν ²	$\frac{3.3462 + 70.8 \times 10^{-12} \nu^2}{2.7692 - 47.2 \times 10^{-12} \nu^2}$	15453- 21838	<i>Alms, 1975;</i> <i>Sneep, 2005</i>	300-320, 532	Johnston, 1975; Sneep, 2005
SF ₆	18611.4 + $\frac{8.9566 \times 10^{14}}{1.680 \times 10^{10} - \nu^2}$	1.0	15385- 40000	<i>Sneep, 2005;</i> Vukovic, 1996; <i>Wilmouth, 2020</i>	<i>264-297</i> 333-363, 532, 633	Sneep, 2005; Vukovic, 1996; Wilmouth, 2019, 2020
O ₂ ^a	20564.8 + $\frac{2.480899 \times 10^{13}}{4.09 \times 10^9 - \nu^2}$	1.09 + 1.385 × 10 ⁻¹¹ ν ² + 1.448 × 10 ⁻²⁰ ν ⁴	18315- 34722	<i>Bates 1984;</i> Hohm, 1993; <i>Sneep, 2005</i>	328-667	Thalman, 2013; Jordan, 2019; Hermans, 1999; Greenblatt, 1990; Spiering, 2011

删除的内容: Thalman

删除的内容: 2014

带格式的: 字体: 加粗, 倾斜

带格式的: 字体: 加粗

带格式的: 字体: 加粗, 倾斜

带格式的: 字体: 倾斜

带格式的: 字体: 加粗

带格式的: 字体: 倾斜

带格式的: 字体: 加粗

带格式的: 字体: 加粗, 倾斜

带格式的: 字体: 倾斜

带格式的: 字体: 加粗

带格式的: 字体: 加粗

带格式的: 字体: 倾斜

751 Unless noted, the refractive index is scaled to 288.15 K and 1013.25 hPa. N = 2.546899 × 10¹⁹
 752 molecules cm⁻³.

753 Due to limited space, only the first name of each reference is shown in the table.

754 **The references in bold and italics describe the formulation of refractive index and King correction**
 755 **factor for n-based calculation, respectively.**

756 ^a The refractive index was obtained at 273.15 K and 1013.25 hPa, N = 2.68678 × 10¹⁹ molecules
 757 cm⁻³ is used in Eq. (1)

760 Table 2. The Rayleigh scattering cross sections (10^{-27} cm²) calculated from the refractive index
 761 (*n*-based) and obtained from BBCES (Exp) of selected wavelengths.

删除的内容: cross-sections

$\lambda(\text{nm})$	CO ₂		SF ₆		N ₂ O		O ₂		CH ₄	
	<i>n</i> -based	Exp	<i>n</i> -based	Exp	<i>n</i> -based	Exp	<i>n</i> -based	Exp	<i>n</i> -based	Exp
330	98.22	96.8	241.5	239.4	137.9	136.7	34.71	35.1	84.12	85.3
404	41.67	41.6	104.5	105.7	57.71	57.9	14.57	14.8	35.57	35.9
532	13.32	13.3	33.92	34.1	18.19	18.3	4.642	4.55	11.34	11.3
660	5.516	5.52	14.16	14.2	7.483	7.47	1.924	1.95	4.693	4.68
710	4.101	4.08	10.55	10.4	5.551	5.48	1.430	1.41	3.487	3.47

762

764 **References**

- 765 [Abjean, R., Mehu, A., and A. J.: Interferometric measurement of refraction indices of helium and](#)
766 [neon in ultra violet, *Comptes Rendus Hebdomadaires des Seances de l Academie des*](#)
767 [Sciences Serie B, 271, 835-&, 1970.](#)
- 768 [Adel, A. and Slipher, V. M.: The Constitution of the Atmospheres of the Giant Planets, *Phys. Rev.*,](#)
769 [46, 902-906, 10.1103/PhysRev.46.902. 1934.](#)
- 770 Alms, G. R., Burnham, A. K., and Flygare, W. H.: Measurement of the dispersion in polarizability
771 anisotropies, *J. Chem. Phys.*, 63, 3321-3326, 10.1063/1.431821, 1975.
- 772 Baidar, S., Oetjen, H., Coburn, S., Dix, B., Ortega, I., Sinreich, R., and Volkamer, R.: The CU
773 Airborne MAX-DOAS instrument: vertical profiling of aerosol extinction and trace gases,
774 *Atmos. Meas. Tech.*, 6, 719-739, 10.5194/amt-6-719-2013, 2013.
- 775 [Bates RD. Rayleigh scattering by air. *Planet Space Sci.*, 32:785–90, 10.1016/0032-](#)
776 [0633\(84\)90102-8, 1984:](#)
- 777 Bates, D. R., and Hays, P. B.: Atmospheric nitrous oxide, *Plan. Space Sci.*, 15, 189-197,
778 10.1016/0032-0633(67)90074-8, 1967.
- 779 Bideau-Mehu, A., Guern, Y., Abjean, R., and Johannin-Gilles, A.: Interferometric determination
780 of the refractive index of carbon dioxide in the ultraviolet region, *Opt. Commun.*, 9, 432-434,
781 10.1016/0030-4018(73)90289-7, 1973.
- 782 Bluvshstein, N., Flores, J. M., Segev, L., and Rudich, Y.: A new approach for retrieving the UV-
783 vis optical properties of ambient aerosols, *Atmos. Meas. Tech.*, 9, 3477-3490, 10.5194/amt-
784 9-3477-2016, 2016.
- 785 Bluvshstein, N., Lin, P., Flores, J. M., Segev, L., Mazar, Y., Tas, E., Snider, G., Weagle, C., Brown,
786 S. S., Laskin, A., and Rudich, Y.: Broadband optical properties of biomass-burning aerosol
787 and identification of brown carbon chromophores, *J. Geophys. Res. Atmos.*, 122, 5441-5456,
788 10.1002/2016JD026230, 2017.
- 789 Cuthbertson, C., and Cuthbertson, M.: On the refraction and dispersion of carbon dioxide, carbon
790 monoxide, and methane, *Proc. R. Soc. Lond. A*, 97, 152-159, 10.1098/rspa.1920.0020, 1920.
- 791 Cuthbertson, C., and Cuthbertson, M.: The refraction and dispersion of neon and helium, *Proc. R.*
792 *Soc. Lond. A*, 135, 40-47, 10.1098/rspa.1932.0019, 1932.
- 793 Drouin, B. J., Benner, D. C., Brown, L. R., Cich, M. J., Crawford, T. J., Devi, V. M., Guillaume,
794 A., Hodges, J. T., Mlawer, E. J., Robichaud, D. J., Oyafuso, F., Payne, V. H., Sung, K.,
795 Wishnow, E. H., and Yu, S.: Multispectrum analysis of the oxygen A-band, *J. Quant.*
796 *Spectrosc. Radiat. Transf.*, 186, 118-138, 10.1016/j.jqsrt.2016.03.037, 2017.
- 797 Fink, U., Benner, D. C., and Dick, K. A.: Band model analysis of laboratory methane absorption
798 spectra from 4500 to 10500 Å, *J. Quant. Spectrosc. Radiat. Transf.*, 18, 447-457,
799 10.1016/0022-4073(77)90077-2, 1977.
- 800 Fuchs, H., Dube, W. P., Lerner, B. M., Wagner, N. L., Williams, E. J., and Brown, S. S.: A
801 Sensitive and Versatile Detector for Atmospheric NO₂ and NO_x Based on Blue Diode Laser
802 Cavity Ring-Down Spectroscopy, *Environ. Sci. Technol.*, 43, 7831-7836, 10.1021/es902067h,
803 2009.
- 804 Giver, L. P.: Intensity measurements of the CH₄ bands in the region 4350 Å to 10,600 Å, *J. Quant.*
805 *Spectrosc. Radiat. Transf.*, 19, 311-322, 10.1016/0022-4073(78)90064-X, 1978.
- 806 Gordon, I. E., Rothman, L. S., Hill, C., Kochanov, R. V., Tan, Y., Bernath, P. F., Birk, M., Boudon,
807 V., Campargue, A., Chance, K. V., Drouin, B. J., Flaud, J. M., Gamache, R. R., Hodges, J.
808 T., Jacquemart, D., Perevalov, V. I., Perrin, A., Shine, K. P., Smith, M. A. H., Tennyson, J.,

809 Toon, G. C., Tran, H., Tyuterev, V. G., Barbe, A., Császár, A. G., Devi, V. M., Furtenbacher,
810 T., Harrison, J. J., Hartmann, J. M., Jolly, A., Johnson, T. J., Karman, T., Kleiner, I., Kyuberis,
811 A. A., Loos, J., Lyulin, O. M., Massie, S. T., Mikhailenko, S. N., Moazzen-Ahmadi, N.,
812 Müller, H. S. P., Naumenko, O. V., Nikitin, A. V., Polyansky, O. L., Rey, M., Rotger, M.,
813 Sharpe, S. W., Sung, K., Starikova, E., Tashkun, S. A., Auwera, J. V., Wagner, G., Wilzewski,
814 J., Wcisło, P., Yu, S., and Zak, E. J.: The HITRAN2016 molecular spectroscopic database, *J.*
815 *Quant. Spectrosc. Radiat. Transf.*, 203, 3-69, <https://doi.org/10.1016/j.jqsrt.2017.06.038>,
816 2017.

817 Greenblatt, G. D., Orlando, J. J., Burkholder, J. B., and Ravishankara, A. R.: Absorption
818 measurements of oxygen between 330 and 1140 nm, *J. Geophys. Res. Atmos.*, 95, 18577-
819 18582, 10.1029/JD095iD11p18577, 1990.

820 He, Q., Bluvshstein, N., Segev, L., Meidan, D., Flores, J. M., Brown, S. S., Brune, W., and Rudich,
821 Y.: Evolution of the Complex Refractive Index of Secondary Organic Aerosols during
822 Atmospheric Aging, *Environ. Sci. Technol.*, 52, 3456-3465, 10.1021/acs.est.7b05742, 2018.

823 Hermans, C., Vandaele, A. C., Carleer, M., Fally, S., Colin, R., Jenouvrier, A., Coquart, B., and
824 Mérianne, M.-F.: Absorption cross-sections of atmospheric constituents: NO₂, O₂, and H₂O,
825 *Environ. Sci. Pollut. Res.*, 6, 151-158, 10.1007/BF02987620, 1999.

826 Herron, J. P.: Rayleigh-Scatter Lidar Observations at USU's Atmospheric Lidar Observatory
827 (Logan,UT) - Temperature Climatology, Temperature Comparisons with MSIS, and
828 Noctilucent Clouds, Doctor of Philosophy (PhD), Utah State University, 2007.

829 Hohm, U.: Experimental determination of the dispersion in the mean linear dipole polarizability
830 $\alpha(\omega)$ of small hydrocarbons and evaluation of Cauchy moments between 325 nm and 633 nm,
831 *Mol. Phys.*, 78, 929-941, 10.1080/00268979300100621, 1993.

832 Ityakov, D., Linnartz, H., and Ubachs, W.: Deep-UV Rayleigh scattering of N₂, CH₄ and SF₆,
833 *Mol. Phys.*, 106, 2471-2479, 10.1080/00268970802570334, 2008a.

834 Ityakov, D., Linnartz, H., and Ubachs, W.: Deep-UV absorption and Rayleigh scattering of carbon
835 dioxide, *Chem. Phys. Lett.*, 462, 31-34, 10.1016/j.cplett.2008.07.049, 2008b.

836 Johnston, H. S., and Selwyn, G. S.: New cross sections for the absorption of near ultraviolet
837 radiation by nitrous oxide (N₂O), *Geophys. Res. Lett.*, 2, 549-551,
838 10.1029/GL002i012p00549, 1975.

839 Jordan, N., Ye, C. Z., Ghosh, S., Washenfelder, R. A., Brown, S. S., and Osthoff, H. D.: A
840 broadband cavity-enhanced spectrometer for atmospheric trace gas measurements and
841 Rayleigh scattering cross sections in the cyan region (470–540 nm), *Atmos. Meas.*
842 *Tech.*, 12, 1277-1293, 10.5194/amt-12-1277-2019, 2019.

843 King, L. V., and Eve, A. S.: On the complex anisotropic molecule in relation to the dispersion and
844 scattering of light, *Proc. R. Soc. Lond. A*, 104, 333-357, 10.1098/rspa.1923.0113, 1923.

845 Leonard, P. J.: Refractive indices, Verdet constants, and Polarizabilities of the inert gases, *At. Data*
846 *Nucl. Data Tables*, 14, 21-37, 10.1016/s0092-640x(74)80028-8, 1974.

847 Long, C. A., and Ewing, G. E.: Spectroscopic investigation of van der Waals molecules. I. The
848 infrared and visible spectra of (O₂)₂, *J. Chem. Phys.*, 58, 4824-4834, 10.1063/1.1679066,
849 1973.

850 Min, K. E., Washenfelder, R. A., Dube, W. P., Langford, A. O., Edwards, P. M., Zarzana, K. J.,
851 Stutz, J., Lu, K., Rohrer, F., Zhang, Y., and Brown, S. S.: A broadband cavity enhanced
852 absorption spectrometer for aircraft measurements of glyoxal, methylglyoxal, nitrous acid,
853 nitrogen dioxide, and water vapor, *Atmos. Meas. Tech.*, 9, 423-440, 10.5194/amt-9-423-2016,
854 2016.

855 Naus, H., and Ubachs, W.: Experimental verification of Rayleigh scattering cross sections, *Opt.*
856 *Lett.*, 25, 347-349, 10.1364/OL.25.000347, 2000.

857 Newnham, D. A., and Ballard, J.: Visible absorption cross sections and integrated absorption
858 intensities of molecular oxygen (O₂ and O₄), *J. Geophys. Res. Atmos.*, 103, 28801-28815,
859 10.1029/98JD02799, 1998.

860 Platt, U., and Stutz, J.: Differential Optical Absorption Spectroscopy, in: *Physics of Earth and*
861 *Space Environments*, Springer Berlin Heidelberg, 2008.

862 Shardanand, S., and Rao, A. D. P.: Absolute Rayleigh scattering cross sections of gases and freons
863 of stratospheric interest in the visible and ultraviolet regions, NASA Technical Note, 1977.

864 Smith, W. H., Conner, C. P., and Baines, K. H.: Absorption-Coefficients for the 6190-a Ch₄-Band
865 between 290-Degrees-K and 100-Degrees-K with Application to Uranus Atmosphere, *Icarus*,
866 85, 58-64, 10.1016/0019-1035(90)90103-G, 1990.

867 Sneep, M., and Ubachs, W.: Direct measurement of the Rayleigh scattering cross section in various
868 gases, *J. Quant. Spectrosc. Ra.*, 92, 293-310, 10.1016/j.jqsrt.2004.07.025, 2005.

869 Spiering, F. R., Kiseleva, M. B., Filippov, N. N., van Kesteren, L., and van der Zande, W. J.:
870 Collision-induced absorption in the O₂ B-band region near 670 nm, *Phys. Chem. Chem. Phys.*,
871 13, 9616-9621, 10.1039/C1CP20403C, 2011.

872 Strutt, J. W.: XXXIV. On the transmission of light through an atmosphere containing small
873 particles in suspension, and on the origin of the blue of the sky, London, Edinburgh Dublin
874 *Philos. Mag. J. Sci.*, 47, 375-384, 10.1080/14786449908621276, 1899.

875 Strutt, R. J.: The light scattered by gases: its polarisation and intensity, *Proc. R. Soc. Lond. A*, 95,
876 155-176, 10.1098/rspa.1918.0057, 1918.

877 Strutt, R. J.: A re-examination of the light scattered by gases in respect of polarisation. I-
878 Experiments on the common gases, *Proc. R. Soc. Lond. A*, 97, 435-450,
879 10.1098/rspa.1920.0044, 1920.

880 Thalman, R., and Volkamer, R.: Temperature dependent absorption cross-sections of O₂-O₂
881 collision pairs between 340 and 630 nm and at atmospherically relevant pressure, *Phys. Chem.*
882 *Chem. Phys.*, 15, 15371-15381, 10.1039/C3CP50968K, 2013.

883 Thalman, R., Zarzana, K. J., Tolbert, M. A., and Volkamer, R.: Rayleigh scattering cross-section
884 measurements of nitrogen, argon, oxygen and air, *J. Quant. Spectrosc. Radiat. Transf.*, 147,
885 171-177, 10.1016/j.jqsrt.2014.05.030, 2014.

886 [Thalman, R., Zarzana, K. J., Tolbert, M. A., and Volkamer, R.: Erratum to "Rayleigh scattering](#)
887 [cross-section measurements of nitrogen, argon, oxygen and air" J. Quant. Spectrosc. Radiat.](#)
888 [Transf., 147 \(2014\) 171-177, J. Quant. Spectrosc. Radiat. Transf., 189, 281-282,](#)
889 [10.1016/j.jqsrt.2016.12.014, 2017.](#)

890 Tomasi, C., Vitale, V., Petkov, B., Lupi, A., and Cacciari, A.: Improved algorithm for calculations
891 of Rayleigh-scattering optical depth in standard atmospheres, *Appl. Opt.*, 44, 3320-3341,
892 10.1364/AO.44.003320, 2005.

893 Vukovic, D., Woolsey, G. A., and Scelsi, G. B.: Refractivities of and at wavelengths of 632.99 and
894 1300 nm, *Journal of Physics D: Applied Physics*, 29, 634-637, 10.1088/0022-3727/29/3/023,
895 1996.

896 Washenfelder, R. A., Langford, A. O., Fuchs, H., and Brown, S. S.: Measurement of glyoxal using
897 an incoherent broadband cavity enhanced absorption spectrometer, *Atmos. Chem. Phys.*, 8,
898 7779-7793, 10.5194/acp-8-7779-2008, 2008.

- 899 Washenfelder, R. A., Flores, J. M., Brock, C. A., Brown, S. S., and Rudich, Y.: Broadband
900 measurements of aerosol extinction in the ultraviolet spectral region, *Atmos. Meas. Tech.*, 6,
901 861-877, 10.5194/amt-6-861-2013, 2013.
- 902 Washenfelder, R. A., Attwood, A. R., Flores, J. M., Zarzana, K. J., Rudich, Y., and Brown, S. S.:
903 Broadband cavity-enhanced absorption spectroscopy in the ultraviolet spectral region for
904 measurements of nitrogen dioxide and formaldehyde, *Atmos. Meas. Tech.*, 9, 41-52,
905 10.5194/amt-9-41-2016, 2016.
- 906 Watson, H. E., and Ramaswamy, K. L.: The refractive index dispersion and polarization of gases,
907 *Proceedings of the Royal Society of London. Series A - Mathematical and Physical Sciences*,
908 156, 144-157, 10.1098/rspa.1936.0140, 1936.
- 909 Wilmouth, D. M., and Sayres, D. S.: Rayleigh scattering cross sections of argon, carbon dioxide,
910 sulfur hexafluoride, and methane in the UV-A region using Broadband Cavity Enhanced
911 Spectroscopy, *J. Quant. Spectrosc. Radiat. Transf.*, 234, 32-39, 10.1016/j.jqsrt.2019.05.031,
912 2019.
- 913 Wilmouth, D. M., and Sayres, D. S.: Determination of Rayleigh scattering cross sections and
914 indices of refraction for Ar, CO₂, SF₆, and CH₄ using BBCES in the ultraviolet, *J. Quant.*
915 *Spectrosc. Radiat. Transf.*, 107224, 10.1016/j.jqsrt.2020.107224, 2020.